PUMPENTAGUNG
PUMP CONGRESS
KARLSRUHE '92
06. bis 08. OKTOBER 1992

PREPRINT

A 1-04

Sektion A 1 Kraftwerke
Section A 1 Power stations

Dr. S. Gopalakrishnan

BW/IP INTERNATIONAL, INC.
Los Angeles, CA 90058 / USA

Analytical Investigation of Thermal Cracking in Reactor Recirculating Pumps

Eine analytische Untersuchung der thermischen Rißbildung in Umwalzpumpen

1.0 INTRODUCTION

Byron Jackson boiling water recirculation pumps, (see Figure 1.1), have provided many years of reliable, trouble-free service. In the early 1980s, however, significant linear indications (shallow cracks) began to appear in the thermal barrier area of these units. These were observed both on the shaft and in the cover bore in a region extending one inch axially into the thermal barrier to approximately one inch below the barrier. Subsequent in-service inspections have shown that most BWR recirculation pumps are affected. Crack depths range in magnitude from mils to fractions of an inch on both the cover and the shafting. Fractographic examination of the cracked shaft surfaces and analytical studies have convincingly shown that these cracks propagate as a result of thermal cycling fatigue. In these pumps a part of seal injection water (about 2 gpm) flows down the annulus between the shaft and the thermal barrier and mixes with the system water. It is this mixing that causes alternating temperatures on the metal surfaces and they lead to thermal cyclic fatigue.

Several recirculating pumps of boiling water reactors have been disassembled after many years of service, and some observations have been made regarding the cracks:

On the shaft, the cracks are predominantly axial, even though in some areas they tend to coalesce and become circumferential in orientation. Axial cracks tend to be shallow (less than 1/4" deep), whereas circumferential cracks grow deeper. In one BWR6 plant, the hollow pump shaft had through-the-wall cracks. Metallographic studies have indicated no environmental influence or shaft material abnormality. On the cover, the cracks are entirely axial and shallow. However, because of proximity of clean cooling water holes in the vicinity, concern exists regarding the possibility of system water seeping into these holes and contaminating the clean water system.

This paper will summarize the key results of a great deal of research that has been conducted to understand the origin of cracks and their propagation tendencies and to develop suitable countermeasures.

2.0 ANALYSIS

The temperature and velocity fields in the annulus are very complex because of the interaction of several phenomena:

i. The Taylor-Couette flow in the annulus formed by a rotating inner cylinder and a stationary outer cylinder.

ii. A superimposed small axial flow.

iii. An axial imposed temperature gradient since the injection water is substantially cooler than the reactor system water.

iv. Other externally imposed pressure fluctuations.

In order to make a parametric analysis possible, it is important to establish whether dominant frequencies in the temperature field are likely to exist in comparison to broad band or random components only. Ignoring for the moment the contributions due to item (iv) above, a fundamental research work is underway (Ref. 1) to develop basic knowledge regarding the temperature and velocity spectra. It is well known that for a pure Taylor-Couette flow, at a critical Taylor number (= 1700), Taylor vortices are formed. Axial flow suppresses the formation of the Taylor vortices and hence the critical T_a increases to about 10^5 for axial Reynolds number (R_a) of about 2000. It is also known that vortices persist for rotational Reynolds number (R_w) values well in excess of the R_w corresponding to the critical T_a. The presence of axial temperature gradients further complicates the phenomena. Preliminary work (Ref. 1) indicates that the temperature spectrum does contain dominant frequencies much lower than rotational speed. Since the tests of Reference 1 have not yet duplicated actual R_a, T_a and Grashof numbers, general conclusions can not be drawn. However, it appears reasonable to suggest that frequency components from about 10% to 100% of rotating speed may exist in the actual temperature and velocity field. This contention is strengthened if we include item (iv), where once per rev. and subharmonic frequencies can certainly be expected to exist. Therefore, a basic premise was made that the thermal mixing can be simulated by imposing a cyclic fluctuation of the axial flow driving force, namely the pressure differential from the top to the bottom of the annulus.

2.1 Transient Flow and Heat Transfer Analysis

The thermal barrier area is modelled as an axi-symmetric annulus surrounded by axi-symmetric rings representing the shaft-and-cover as shown in Figure 2.1. The radial thickness of the shaft and cover is restricted to be 0.25" as it can be shown that even at low frequencies, the penetration of the temperature field is not significant beyond this depth. The boundary conditions of pressure and temperature are indicated. The velocity of water at any point will vary with time as shown typically in Figure 2.1. Assuming that the flow is incompressible, one can show that at any instant of time the velocity is the same at any point in the annulus. From time t_1 to t_2, the velocity is negative and during this period, the hot water will move up the annulus. The maximum penetration distance Z_{max} is given by integrating the velocity from time t_1 to t_2.

The equation governing the variation in axial velocity U through the gap can be stated as below:

$$\rho \frac{\partial U}{\partial t} + f_r \frac{1}{2 D_h} \rho U|U| = - \frac{\partial p}{\partial x} - \frac{P_1 - \bar{P}_2 - \Delta P \sin (2\pi ft)}{L}$$

with $f_r = \dfrac{0.94}{|U|^{0.659}}$, as derived in Section 2.2.

The above equation can be solved numerically for each incremental time step. At the conclusion of one period, the resulting U is compared with the assumed U value at start. If they are not equal, the process is repeated until convergence. The analyses were carried out for several cases of flow rate, frequency and ΔP.

The maximum penetration distance for the case of $\Delta P = 2.5$ psi is shown in Figure 2.2. It can be seen that for any frequency, the maximum penetration distance Z_{max} decreases with flow rate and beyond about 4 gpm, Z_{max} is zero. For any given flow, Z_{max} increases as f decreases.

For the heat transfer analysis, separate differential equations and boundary conditions are set up for water, shaft and cover as below:

Water

$$\rho_w c_w \frac{\partial T_w}{\partial t} + \rho_w c_w U \frac{\partial T_w}{\partial x} = \frac{2h_c}{D_h} (T_c - T_w)$$

$$+ \frac{2h_s}{D_h} (T_s - T_w) + k_t \frac{\partial^2 T_w}{\partial x^2}$$

The appropriate boundary conditions for water are:

if $U > 0$, $T_w\big|_{x=0} = 100°F$; if $U < 0$, $T_w\big|_{x=L} = 550°F$

The determination of the heat transfer coefficients is described in Section 2.2.

Cover

$$\frac{\partial T_c}{\partial t} = \alpha_c \left(\frac{\partial^2 T_c}{\partial x^2} + \frac{\partial^2 T_c}{\partial y^2}\right)$$

at $y = 0$, $- k_c \frac{\partial T_c}{\partial y} = h_c (T_c - T_w)$

and at $y = b_c$ $\qquad T_c = 120°F \quad 0 \leq x \leq L$

Shaft

$$\frac{\partial T_s}{\partial t} = \alpha_s \left(\frac{\partial^2 T_s}{\partial x^2} + \frac{\partial^2 T_s}{\partial y^2}\right)$$

$$\text{at } y = 0, \; -k_s \frac{\partial T_s}{\partial y} = h_s (T_s - T_w)$$

$$\text{and at } y = b_s, \quad \frac{\partial T_s}{\partial y} = 0$$

The equations were discretized using a finite difference approximation and the resulting algebraic equations were solved using TDMA algorithm described in Reference 2.

For each of the cases studied, temperature of the fluid and shaft and cover surfaces were obtained as a function of time. The maximum cyclic temperature variation can then be plotted as a function of the axial distance (Figure 2.3).

2.2 Estimation of Friction Factor and Heat Transfer Coefficients

The momentum and energy equations for the groove geometry were solved using an axi-symmetric finite difference algorithm (Reference 3). The flow was taken to be incompressible and the K-E turbulence model was used. Each periodic passage was represented by a 50x54 grid.

To verify the solution method, the technique was first applied on a geometry for which test data (Ref. 4) have been published. Figure 2.4 shows the variation of friction factor with Reynolds number for Yamada's geometry. The test data of Yamada compares very well with the calculations, for all three rotational Reynolds numbers. Figure 2.4 also shows the predicted curve for the existing geometry shown as a dotted line ($R_w = 40{,}000$). From a curve fit of the dotted line, friction factor can be expressed analytically as a function of the axial velocity.

The heat transfer coefficient calculations were also made using the same model by using wall heat flux predictions and the calculated log mean temperature difference of the fluid passing through one geometric period of the groove orientations.

To further verify if the above calculated numbers are reasonable, an experiment was conducted using the analogy between mass and heat transfer. A model of the annulus was

made in which the grooving details were accurately represented. The model was coated with Naphthalene, and blowing air through it, Naphthalene was allowed to sublimate. Measuring the loss of mass, it was possible to obtain values of modified Nusselt Number. The experiment was conducted for a range of rotational and axial Reynolds numbers.

In Figure 2.4 the friction coefficients obtained from the sublimation test are also shown, and reasonable correspondence with data of Ref. 4 and the calculations is seen. Similar agreement was also obtained for the heat transfer coefficient.

2.3 Crack Propagation Analysis for Cover

Steady-state stresses were calculated using the ANSYS progrma on a large finite element model consisting of the pump shaft, cover, and parts of the pump case and motor mount. To calculate the alternating stresses, a small portion of the relevant area of the cover was modelled in a much greater detail.

The stress intensity factors corresponding to the calculated distributions of alternating hoop stress were estimated by piecewise summation of a basic point load stress intensity equation. The variations of ΔK along the direction of crack propagation are given in Figure 2.5 for net flow down the annulus of 0.5 gpm. From this, the crack growth rate can be determined by integrating the well-known crack growth equation (Paris Law).

Figure 2.6 shows the rate at which cracks can be expected to grow in time. The results are shown for 2.0 gpm and 0.5 gpm net down-flow, and at two frequencies - 2 Hz, and 1 Hz. The amplitude of pressure pulsation was 2.5 psi and 1 psi. On each curve, the maximum crack depth is indicated for assumed ΔK_{th} values of 3 and 5 ksi/in. On this figure, the maximum crack depths measured in field pumps are also shown. The predictions for 2.0 gpm, 2.5 psi, 1 Hz and 0.5 gpm, 1 psi, 2 Hz appear to bound the measurements.

It is interesting to observe that the crack depths are predicted to be smaller with the lower injection rate. The reason is that in this case, the upward penetration of the hot water is deeper, but there is more time and distance to cause a smearing of the temperature gradient resulting in lower alternating stresses. Based on this finding and other mock-up tests, the net down flow was reduced in field pumps from about 3 gpm to less than 1 gpm. The measured crack depths were of the order of about 1/4" which coincide with the predicted value by this paper. No seepage of system water into the component cooling water has been observed.

No crack potential is observed for frequencies greater than 5 Hz. This finding is corroborated by the results of crack surface striations which indicate 0.5 Hz to 1 Hz exciting frequencies.

2.4 Crack Propagation Analysis for Shaft

The calculation procedure for the shaft is very similar to that for the cover. The resulting stress distribution and stress intensity factor variation with depth are nearly the same as for the cover. Hence these details are not presented in this paper. The final results of crack depth versus time are shown in Figure 2.7. Only two curves corresponding to 2 gpm / 2.5 psi and 0.5 gpm / 1 psi, both at 2 Hz are shown as being representative of all the parametric calculations.

The axial crack depths measured in the field pump are also shown. Majority of the points fall along the prediction lines. However, a few points fall significantly below the predictions implying that the frequency was significantly higher. In Reference 5, a simplified method for shaft crack calculation was adopted based on a quasi-steady assumption of the temperature field. Calculations were performed for 2.5 Hz and 25 Hz (representing once per rev. in many installations) and these results bound the field data quite well.

In the field, both axial and circumferential cracks were observed, the latter being deeper in most cases. Since the circumferential cracks can be driven by mechanical loads, they can be expected to be deeper than axial cracks. Since the present paper does not deal with propagation due to mechanical loads, these field data are not shown in Figure 2.7. Reference 5 shows these data points along with certain scenarios of growth due to mechanical loads.

3.0 COUNTERMEASURES

Based on the research work done to date and field observations, a two-phase strategy has been adopted as countermeasure to the cracking problem. The first phase applies to installations which have reached a number of operating hours at which it was considered prudent to conduct an in-service inspection. For these installations, new components of the same basic design, but with some significant improvements were offered (Ref. 5). These upgrades, by themselves, do not eliminate the mechanism for thermal cracking, but provide a greater margin for safe operation in combination with reduced purge flow operation.

The second phase in this program is the development of a permanent countermeasure which will substantially eliminate the thermal cracking mechanism. The basis for this concept, as described in Reference 6, is the elimination of the temperature differential between the mixing streams by elevating the temperature of the purge flow after emerging from the seal cavity and just prior to mixing with the system water. The concept has been fully tested in mock-up arrangements and other configurations in Japan. It is scheduled to be installed at a new plant in the near future.

4.0 CONCLUSIONS

1. The thermal cracks observed on the shaft and cover of Byron Jackson reactor recirculating pumps are initiated by thermal mixing between the cold injection water and hot system water.

2. An analysis has been developed based on the premise that thermal mixing can be simulated by imposing pressure fluctuations of suitable frequency and amplitude. These result in thermal cycling as the hot water is alternately drawn into and out of the thermal barrier.

3. The predicted crack depths are compared to field observations for the shaft and cover. Significant scatter exists on the field data but they are bounded by reasonable assumptions for frequency and amplitude of pulsations in pressure.

4. A permanent countermeasure which will substantially eliminate the thermal cracking problem has been developed and has just completed final verification tests. It will be offered for installation in the very near future.

5.0 NOMENCLATURE

b	Radial gap of annulus
b_s	Radial depth of shaft used in mathematic model
b_c	Radial depth of cover used in mathematic model
c_w	Specific heat of water
D_h	Hydraulic diameter of annulus gap
f	Frequency of pressure fluctuations
f_r	Friction coefficient
g	Acceleration due to gravity
h_c	Heat transfer coefficient between water and cover surface
h_s	Heat transfer coefficient between water and shaft surface
k_t	Turbulent conductivity for heat
L	Annulus length
p_1	Pressure at top of annulus
p_2	Mean pressure at bottom of annulus
ΔP	Amplitude of pressure pulsation
Q	Net down flow in annulus
r	Radius of rotating inner cylinder
R_a	Axial Reynolds number = $2bU/\nu$
R_w	Rotational Reynolds number = wrb/ν

T_a	Taylor number - $R_w^2 b/\gamma$
T_w	Temperature of water
t	Time
U	Axial velocity
x	Axial coordinate
y	Radial coordinate
Z_{max}	Maximum upward penetration distance of hot water
α	Thermal diffusivity
λ	Friction coefficient - $\dfrac{\text{Pressure Drop}}{(\frac{L}{2b}) \cdot (\frac{U^2}{2g})}$
ν	Kinematic viscosity
ρ_w	Density of water
ω	Angular velocity of rotation

6.0 REFERENCES

1. A. G. Shih and M. L. Hunt: "The Effect of an Axial Buoyant Injectant on a Taylor-Couette Flow", Submitted to ASME National Heat Transfer Conference, August 9-12, 1992.

2. Patankar, S.V., "Numerical Heat Transfer and Fluid Flow", McGraw-Hill, New York, 1980.

3. FLUENT - Creare Inc., Hanover, N.H., 1984.

4. Yamada, Y., "On the Pressure Loss of Flow Between Rotating Coaxial Cylinder with Rectangular Grooves" Bulletin of J.S.M.E. 5, No. 20, 1962, p. 642-651.

5. Gopalakrishnan, S., Vaghasia, G.,K. and Reimers, C.R., "Crack Propagation in Main Coolant Pumps", submitted to EPRI Fifth International Workshop on Main Coolant Pumps - April 21-24, 1992, Orlando, Florida.

6. Boster, C., Gopalakrishnan, S., Reimers, C.R., and Vaghasia, G.K., "Pump with Seal Purge Heater", Patent Applied for.

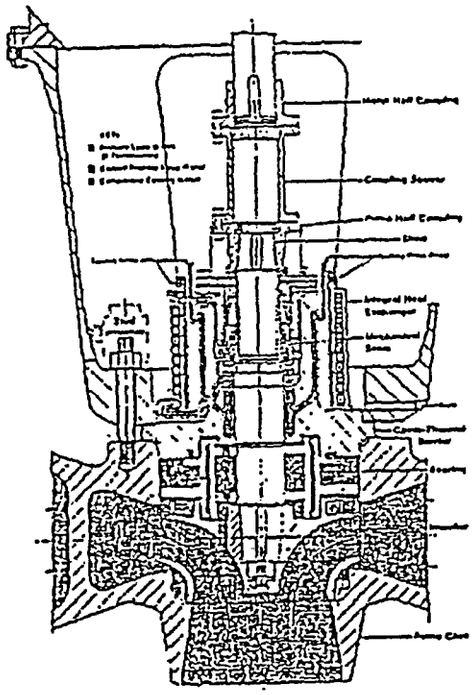

Fig. 1.1 Byron Jackson Nuclear Recirculating Pump

Byron Jackson Umwaelzpumpe

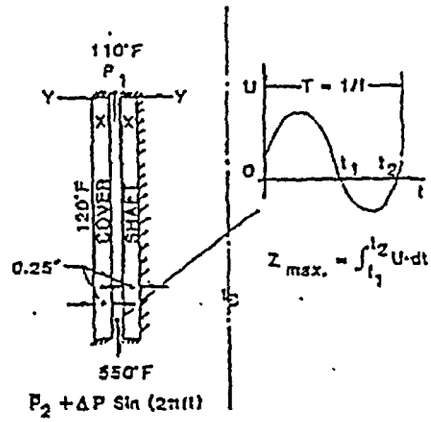

Fig. 2.1 Fluid Mechanics/Heat Transfer Model

Model fuer Hydromechanics/ Waermeaustausch

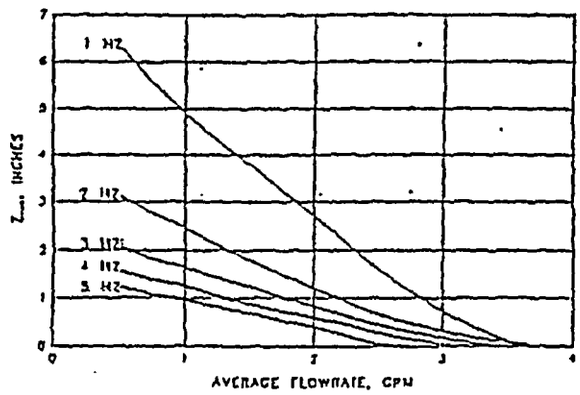

Fig. 2.2 Backflow Penetration Distance $\Delta P = 2.5$ psi

Wirkungstiefe des Rueckflusses $\Delta P = 2.5$ psi

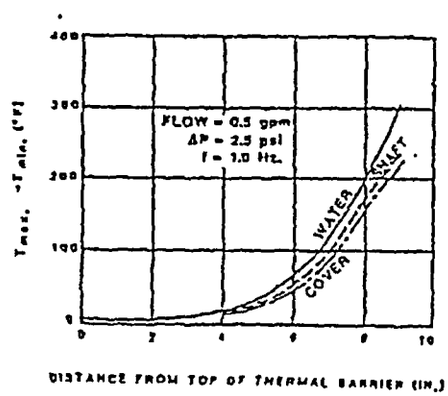

Fig. 2.3 Thermal Barrier Temperature Gradients

Temperatur Profil an der Wellendichtung

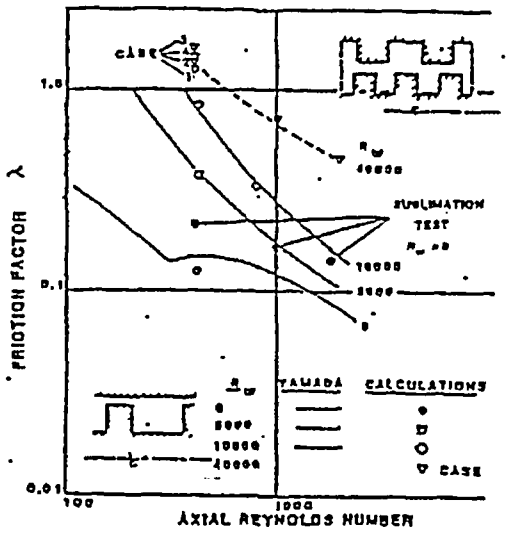

Fig. 2.4 Comparison of Calculated Friction Factor with Data

Vergleich der Berechneten Reibungsfaktoren mit Daten

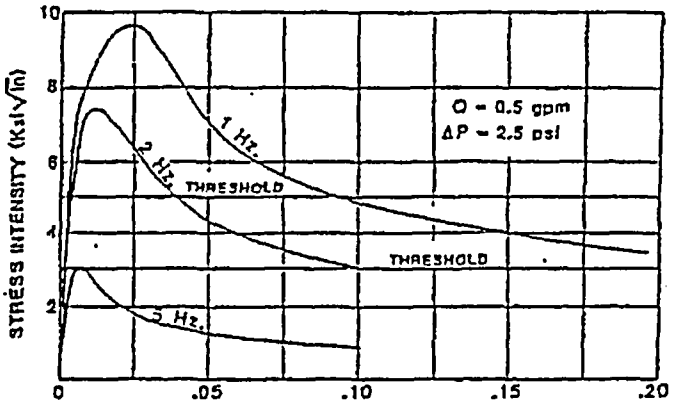

Fig. 2.5 Stress Intensity vs. Crack Depth

Spannung Intensitaet vs. Risstiefe

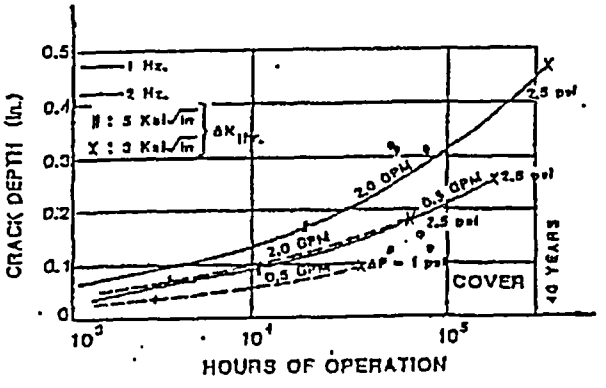

Fig. 2.6 Crack Growth vs. Time

Rissfortschritt vs. Zeit (Deckel)

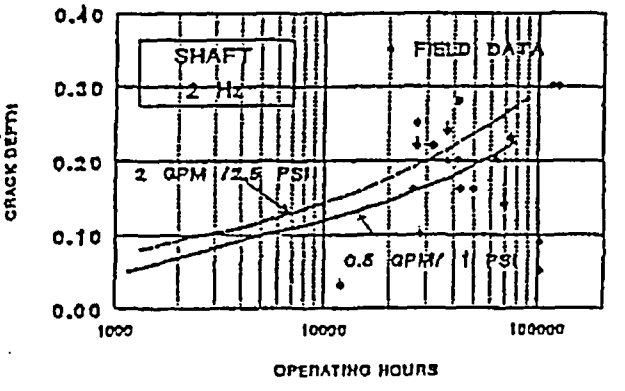

Fig. 2.7 Crack Growth vs. Time

Rissfortschritt vs. Zeit (Welle)